FERMILAB-PUB-07-728-A

arXiv:0708.0871v2 [astro-ph] 25 Nov 2007

Discovery of Four Gravitationally Lensed Quasars from the Sloan Digital Sky Survey

Masamune Oguri,[1,2] Naohisa Inada,[3,4] Alejandro Clocchiatti,[5] Issha Kayo,[6] Min-Su Shin,[2] Joseph F. Hennawi,[7] Michael A. Strauss,[2] Tomoki Morokuma,[4,8] Donald P. Schneider,[9] and Donald G. York[10]

ABSTRACT

We present the discovery of four gravitationally lensed quasars selected from the spectroscopic quasar catalog of the Sloan Digital Sky Survey. We describe imaging and spectroscopic follow-up observations that support the lensing interpretation of the following four quasars: SDSS J0832+0404 (image separation $\theta = 1\farcs98$, source redshift $z_s = 1.115$, lens redshift $z_l = 0.659$); SDSS J1216+3529 ($\theta = 1\farcs49$, $z_s = 2.012$); SDSS J1322+1052 ($\theta = 2\farcs00$, $z_s = 1.716$); and SDSS J1524+4409 ($\theta = 1\farcs67$, $z_s = 1.210$, $z_l = 0.320$). Each system has two lensed images. We find that the fainter image component of SDSS J0832+0404

[1]Kavli Institute for Particle Astrophysics and Cosmology, Stanford University, 2575 Sand Hill Road, Menlo Park, CA 94025.

[2]Princeton University Observatory, Peyton Hall, Princeton, NJ 08544.

[3]Cosmic Radiation Laboratory, RIKEN (The Institute of Physical and Chemical Research), 2-1 Hirosawa, Wako, Saitama 351-0198, Japan.

[4]Institute of Astronomy, Faculty of Science, University of Tokyo, 2-21-1 Osawa, Mitaka, Tokyo 181-0015, Japan.

[5]Pontificia Universidad Católica de Chile, Departamento de Astronomía y Astrofísica, Casilla 306, Santiago 22, Chile.

[6]Department of Physics and Astrophysics, Nagoya University, Chikusa-ku, Nagoya 464-8062, Japan.

[7]Department of Astronomy, University of California at Berkeley, 601 Campbell Hall, Berkeley, CA 94720-3411.

[8]Optical and Infrared Astronomy Division, National Astronomical Observatory of Japan, Mitaka, Tokyo, 181-8588, Japan.

[9]Department of Astronomy and Astrophysics, The Pennsylvania State University, 525 Davey Laboratory, University Park, PA 16802.

[10]Dept. of Astronomy and Astrophysics, and The Enrico Fermi Institute, 5640 So. Ellis Avenue, AAC002, The University of Chicago, Chicago, IL 60637.

is significantly redder than the brighter component, perhaps because of differential reddening by the lensing galaxy. The lens potential of SDSS J1216+3529 might be complicated by the presence of a secondary galaxy near the main lensing galaxy.

Subject headings: gravitational lensing — quasars: general

1. Introduction

Gravitationally lensed multiple quasars provide unique probes of astronomical objects, and are also useful to constrain cosmological parameters. Since gravitational lensing is a pure gravitational effect, it allows us to determine mass distributions of astrophysical objects including dark matter. In addition, the well-known underlying physics makes it a reliable tool to study cosmology. See Kochanek (2006) for a recent review of applications of lensed quasars.

The power of lensed quasars as astrophysical and cosmological probes is enhanced by constructing statistical samples of these objects with well-defined source populations and well-understood selection functions. Statistical lens samples have been constructed in the optical (e.g., Maoz et al. 1993) and the radio (e.g., Helbig et al. 1999) bands. The current largest statistical sample is a radio sample: The Cosmic Lens All-Sky Survey (CLASS; Myers et al. 2003; Browne et al. 2003) discovered 20 lensed quasars among $16,000$ radio sources. The sample has been used to constrain cosmological parameters (e.g., Chae et al. 2002).

The purpose of the Sloan Digital Sky Survey Quasar Lens Search (SQLS; Oguri et al. 2006) is to construct a large statistical lens sample in optical band. The SQLS searches for lensed quasars among spectroscopically confirmed quasar catalogs in the Sloan Digital Sky Survey (SDSS; York et al. 2000). Thus far we have discovered > 20 new lensed quasars as well as several previously known lenses in the SDSS footprint (e.g., Kayo et al. 2007, and references therein), therefore it has already become the largest statistical sample of strongly lensed quasars. Inada et al. (2007) presented the first statistical lens sample of the SQLS from the Data Release 3 (DR3).

In this paper, we report the discoveries of four additional lensed quasars from the SQLS. All the systems are double lenses with small ($1'' - 2''$) image separations. They are initially selected from the SDSS data, and the lensing hypothesis is tested against photometric and spectroscopic follow-up observations at the University of Hawaii 2.2-meter (UH88) telescope, the United Kingdom Infra-Red Telescope (UKIRT), the Subaru telescope, the European

Southern Observatory 3.6-meter (ESO3.6m) telescope, and the Astrophysical Research Consortium 3.5-meter (ARC3.5m) Telescope. We also perform simple mass modeling to further test the validity of their lensing interpretation. Throughout the paper we adopt the standard cosmology with matter density $\Omega_M = 0.27$ and cosmological constant $\Omega_\Lambda = 0.73$. The dimensionless Hubble constant is denoted by h.

2. Selection of Lens Candidates

The aim of the SDSS is to map one quarter of the entire sky by conducting both a photometric survey (Gunn et al. 1998; Lupton et al. 1999; Tucker et al. 2006) in five broad-band optical filters (Fukugita et al. 1996) and a spectroscopic survey with a multi-fiber spectrograph covering 3800 Å to 9200 Å at a resolution of R $\sim$ 1800 (Blanton et al. 2003). The SDSS uses a dedicated 2.5-m telescope (Gunn et al. 2006) at the Apache Point Observatory in New Mexico, USA. The data are processed by automated pipelines (Lupton et al. 2001; Lupton 2007). The targets for spectroscopy are selected based on colors and morphology in the imaging survey (Eisenstein et al. 2001; Richards et al. 2002; Strauss et al. 2002). The astrometry is accurate to better than about $0\farcs1$ rms per coordinate (Pier et al. 2003) and the photometry is calibrated to less than about 0.02 magnitude over the entire survey area (Hogg et al. 2001; Smith et al. 2002; Ivezić et al. 2004). Most of the data are publicly available (Stoughton et al. 2002; Abazajian et al. 2003, 2004, 2005; Adelman-McCarthy 2006, 2007a,b).

Lens systems presented in this paper are selected from the SDSS data using the algorithm described in Oguri et al. (2006). The basic strategy is to select lens candidates from low-redshift ($z < 2.2$) quasars in the SDSS spectroscopic quasar catalogs (e.g., Schneider et al. 2005, 2007). We use two types of selection methods: Morphological selection, designed to locate small-separation ($\sim 1''$) lens candidates, and color selection, to identify lenses with larger image separations. The efficiency of our lens selection is $\sim 10\%$ at small ($\theta < 2''$) image separations (Oguri et al. 2006; Inada et al. 2007). We summarize the SDSS properties of our new lenses in Table 1. The SDSS images of these four candidates are shown in Figure 1. Two of them, SDSS J0832+0404 and SDSS J1216+3529, are selected by the color selection algorithm, whereas the other two are identified by the morphological selection algorithm.

3. Follow-Up Observations of Individual Objects

3.1. SDSS J0832+0404

Optical (V and I) images of SDSS J0832+0404 were taken with the Tektronix 2048×2048 CCD camera (Tek2k; the pixel scale is $0\farcs2195$ pixel^{-1}) at the UH88 telescope on 2006 Nov 15. The seeing was $\sim 1\farcs1$. Images with a total exposure time for each filter of 600 sec were taken under photometric conditions. The fluxes were calibrated using the standard star SA 113 339 (Landolt 1992). We also obtained near-infrared (K) images of this object with the UKIRT Fast-Track Imager (UFTI; the pixel scale is $0\farcs091$ pixel^{-1}) at UKIRT on 2006 October 13. The seeing was $\sim 0\farcs7$, and the total exposure time was 1080 sec. The flux is calibrated using the standard star P545-C (Persson et al. 1998).

Spectral follow-up observations were carried out with the ESO Faint Object Spectrograph and Camera (EFOSC2) at the ESO3.6m on 2005 December 31. The total exposure time was 1800 sec. The wavelength coverage was 3700 Å to 9300 Å with a spectral dispersion of ~ 5 Å pixel^{-1}. The spatial resolution was $0\farcs31$ pixel^{-1}. We used a grating of 236 lines/mm and a $1\farcs0$ slit. The slit was aligned to observe the two components simultaneously. The spectral resolution was $R \sim 400$. We extracted the spectra using standard IRAF[1] tasks. We calibrate the spectra by matching the summed spectral energy distribution (SED) of the two objects to that of the SDSS spectrum. Since the angular separation between the fainter quasar image and the lensing galaxy is small (see below) we did not separate these two components in studying the spectra.

The results of our follow-up imaging is shown in Figure 2. We fit the system using GALFIT (Peng et al. 2002) with two PSFs plus a galaxy modeled by de Vaucouleurs profile in R and I band images, and two PSFs in V-band image because the galaxy is not bright enough. We adopt nearby stars as PSF templates. Subtracting the two PSFs shows the presence of a red lensing galaxy more clearly. The fits give us the relative position and brightness of each component (image A, image B, and lens galaxy G), which we summarize in Table 2. The image separation between two stellar components is $1\farcs984 \pm 0\farcs008$. The spectra shown in Figure 3 confirm that the two stellar components have broad emission lines (C III] and Mg II) at the same wavelengths, supporting the lensing hypothesis of this system. We note that lensed quasar images (components A and B) have different colors; component B ($V - K \sim 3.1$) is considerably redder than component A ($V - K \sim 2.$). This is probably

[1] IRAF is distributed by the National Optical Astronomy Observatories, which are operated by the Association of Universities for Research in Astronomy, Inc., under cooperative agreement with the National Science Foundation.

because of the differential dust reddening from the lensing galaxy, which is sometimes seen in lensed quasar systems (e.g., Falco et al. 1999).

We also measure the redshift of the lensing galaxy from our follow-up spectrum. The spectrum shown in Figure 4 shows a break at ~ 6600 Å (it is weak because of the contamination from image B) and two adjacent absorption lines that we interpret as the 4000 Å break and Ca H & K lines of an elliptical galaxy. From the Ca H & K lines we determine the lens redshift to be $z = 0.659 \pm 0.001$. The optical-infrared color of the lens galaxy, $I - K \sim 3.3$, is broadly consistent with this spectroscopic redshift (e.g., Nelson et al. 2001).

3.2. SDSS J1216+3529

We obtained optical (V, R, and I) images of SDSS J1216+3529 with the Tek2k at the UH88 telescope on 2007 April 11. The total exposure time was 600 sec in I and 300 sec in V and R. The seeing was $\sim 0\farcs7$. Photometric calibration was performed using the standard star PG0918+029 (Landolt 1992). In addition, near-infrared (H) images were taken with the Near-Infrared Camera/Fabry-Perot Spectrometer (NIC-FPS; the pixel scale is $0\farcs2709$ pixel^{-1}) at the ARC3.5m telescope on 2007 March 7. We obtained a total exposure of 900 sec with $\sim 0\farcs7$ seeing. Since no standard star was observed, we perform the photometric calibration using the Two Micron All Sky Survey (2MASS) data.

The spectra of the two stellar components were obtained with the Wide Field Grism Spectrograph 2 (WFGS2; Uehara et al. 2004) at the UH88 telescope on 2007 May 13. The grating of 300 lines/mm and the $0\farcs9$ slit results in a spectral resolution of $R \sim 700$ covering wavelength from 4300 Å to 10000 Å. The spectral dispersion is ~ 5 Å pixel^{-1}, and the spatial resolution is $0\farcs37$ pixel^{-1}. The exposure time was 5700 sec. The observation was conducted under good seeing ($\sim 0\farcs8$), which makes it rather easy to separate two stellar components. The flux is calibrated by the standard star Feige 34 (Oke 1990) and the data were reduced using IRAF.

We show our results of follow-up imaging in Figure 5 and Table 2. In addition to the main lensing galaxy (named G1), a red galaxy (denoted as G2) is visible north of the system. Thus we fit the system with two PSFs plus two galaxies (except for V-band image in which the galaxies are too faint) to derive the magnitudes and positions. These two galaxies may be physically associated, although the colors are slightly different such that galaxy G2 is bluer than G1. The color $R - I \sim 1.0 - 1.2$ suggests that they are early-type galaxies at $z \sim 0.5$ (Fukugita et al. 1995). The colors of two stellar components A and B are quite similar. They are separated by an angle $\theta = 1\farcs489 \pm 0\farcs004$.

The spectra are shown in Figure 6. Multiple quasar emission lines (C IV, C III], and Mg II) are seen in both components A and B, confirming that these are lensed images of a quasar at $z = 2.012$. Moreover the overall shapes of the spectra are quite similar, as shown in the ratio of the spectra. In addition, there are associated absorptions in C IV emission lines of both components, which further support that these are gravitationally lensed images.

3.3. SDSS J1322+1052

Optical images of SDSS J1322+1052 were taken with the Tek2k at the UH88 telescope on 2007 April 11 (I; the seeing was $\sim 0\farcs7$) and 2007 May 16 (V and R; the seeing was $\sim 0\farcs8$). The exposure time was 480 sec in I and 300 sec in V and R. The observations were conducted under photometric conditions, and we used PG0918+029 and PG1633+099 (Landolt 1992) to derive magnitudes in each image. We took follow-up near-infrared (H) images as well with NIC-FPS at the ARC3.5m telescope on 2007 April 26. The seeing was $\sim 0\farcs9$ and the total exposure time was 1200 sec. Again, magnitudes are estimated using the 2MASS data.

We acquired spectra of this system with the WFGS2 at the UH88 telescope on 2007 May 13. We adopted the same instrument configuration described in §3.2, but with a shorter exposure time of 4500 sec.

Figure 8 presents the follow-up images, and Table 4 summarizes the result of fitting. We identify a lensing galaxy (component G) in the images in all four bands. The color, $V - R \sim 1.5$ and $R - I \sim 0.9$, implies a lens redshift of $z \sim 0.5$. The two stellar components (A and B) have similar colors, but the magnitude difference is quite large, $\Delta I = 1.72$, corresponding to a flux ratio of 0.205. The image separation is $2\farcs001 \pm 0\farcs007$. The spectra shown in Figure 8 confirm that components A and B have similar SEDs: Both components have weak C III] and Mg II lines at the same wavelengths, and the ratio of two spectra is almost constant over a wide wavelength range.

3.4. SDSS J1524+4409

We obtained B, R, and I band images of SDSS J1524+4409 with the Orthogonal Parallel Transfer Imaging Camera (OPTIC; the pixel scale is $0\farcs1374$ pixel^{-1}) at the UH88 telescope on 2006 May 4. The exposure time was 400 sec for each filter and the seeing was $\sim 1\farcs1$. The standard star PG1633+099 was used to calibrate the fluxes (Landolt 1992).

Follow-up images shown in Figure 9 indicate that this system consists of two stellar

components (A and B) and a bright extended component (G). The colors of components A and B are similar, thus these are likely to be lensed images. The bright galaxy G has red colors and is fitted well by a de Vaucouleurs profile. The image separation between A and B is $1\farcs669 \pm 0\farcs020$. See Table 5 for the fitting results.

The spectrum of this system was taken with the Faint Object Camera and Spectrograph (FOCAS; Kashikawa et al. 2002) at the Subaru telescope on 2007 January 22. The 300B grism and SY47 filter were used to take the spectrum in the range from 4700 Å to 9100 Å with the resolution of $R \sim 500$. A long slit with $1''$ width was aligned to observe the two quasar images simultaneously. The spatial resolution was $0\farcs2$ pixel^{-1} because of 2×2 on chip binning. The spectral dispersion after the binning is ~ 2.6 Å pixel^{-1}. The excellent seeing of $\sim 0\farcs6$ allows us to extract spectra of all three components (A, B, and G) in a straightforward way. The total exposure was 900 sec. The spectra were flux calibrated using the standard star G191B2B (Oke 1990).

The spectra are shown in Figure 10. As expected, components A and B have quasar emission lines (Mg II and [O II]) at the same wavelengths and similar overall spectral shapes, confirming that they are lensed images of a quasar at $z = 1.210$. A number of absorption lines in the spectrum of component G indicate that the lens is an early-type galaxy at $z = 0.320 \pm 0.001$. The redshift is in agreement with that expected from the colors (Fukugita et al. 1995).

4. Mass Modeling

We perform mass modeling of each lens system. Since the lack of observational constraints for the new lens systems limits detailed studies of their mass distributions, here we adopt the simplest mass model, which are commonly used in lens studies, to check whether such model can fit the new lenses as well. The lens galaxy is assumed to have a singular isothermal ellipsoid profile parameterized by the Einstein radius $R_{\rm E}$, ellipticity e and the position angle (measured East of North) θ_e. We adopt the positions of the quasar images and lensing galaxies (for SDSS J1216+3529 we consider only galaxy G1 because of the small number of our observational constraints) and the fluxes of the quasar images in either I or K band in Tables 2-5. The number of degrees of freedom of this modeling is zero, therefore we should be able to find models that perfectly fit the observations, as long as the assumed model is reasonable. Fitting is performed using *lensmodel* package (Keeton 2001).

We summarize our results in Table 6. In all models the observables are reproduced well, $\chi^2 \sim 0$, with reasonable best-fit values of ellipticity. The existence of feasible mass models

is further support for the hypothesis that these systems are indeed gravitational lenses. In Table 6 we show total magnifications ($\mu_{\rm tot}$) and expected time delays (Δt) of the best-fit models. The errors on the time delays from mass model uncertainties are $\sim 20\%$ (Oguri 2007).

The mass models also predict velocity dispersions of lens galaxies that can be converted to luminosities using the Faber-Jackson relation. We adopt the relation derived by Rusin et al. (2003) to compute the expected I-band magnitude for each lens system. From the spectroscopic lens redshifts of SDSS J0832+0404 and SDSS J1524+4409, we calculate the expected magnitudes to be $I = 19.4$ and $I = 18.9$, respectively. Given the scatter of the relation, ~ 0.5 mag, both the estimated magnitudes agree with the observed magnitudes of the lens galaxies. For SDSS J1216+3529 and SDSS J1322+1052, we invert the problem and assume the observed lens galaxy magnitudes to compute the expected lens redshifts from the Faber-Jackson relation. We find $z_l \sim 0.55$ for both SDSS J1216+3529 and SDSS J1322+1052. The scatter in the Faber-Jackson relation implies an error of $\Delta z \sim 0.1$. The estimated redshifts are consistent with the results inferred from the colors of the lens galaxies.

Although we were able to fit the systems with a simple singular isothermal ellipsoid model, it is not clear whether this model really represents the true density distribution. Complicated lens potentials could affect lensing statistics (see, e.g., Oguri et al. 2005, for the effect of the lens galaxy environment), and thus it is important to explore the mass distributions further. The current lack of available number of observational constrains prevents us from further examinations, hence additional observations (e.g., the detection of extended lensed host galaxies; see Kochanek et al. 2001) will be helpful in obtaining more detailed lens potentials of the individual lens systems.

5. Summary

We have presented the discoveries of four lensed quasar systems. All were identified as lens candidates on the course of the SQLS, a systematic survey of lensed quasars from SDSS spectroscopic quasars. Imaging and spectroscopic observations have shown that the pairs of stellar images have similar SEDs in each case, and that these systems also show lensing galaxies among the stellar components. The image configurations and image flux ratios were easily reproduced with simple mass models. Below we summarize the properties of the four new lensed quasars:

- SDSS J0832+0404: A two-image lens with an image separation of $\theta = 1\farcs984 \pm 0\farcs008$. The source redshift is $z_s = 1.115 \pm 0.003$, and the lens redshift is $z_l = 0.659 \pm 0.001$.

The fainter component is significantly redder than the brighter component. The I-band flux ratio $f_I \sim 0.22$ is smaller than the limit for our statistical lens sample (Oguri et al. 2006).

- SDSS J1216+3529: A two-image lens with an image separation of $\theta = 1\farcs489 \pm 0\farcs004$ and a source redshift of $z_s = 2.012 \pm 0.002$. There is a secondary galaxy G2 near the main lensing galaxy G1: The rough similarity of their colors suggests that they may be physically associated. The observed colors and magnitude of the lens galaxy as well as mass modeling suggest that the lens redshift is ~ 0.55.

- SDSS J1322+1052: A two-image lens with an image separation of $\theta = 2\farcs001 \pm 0\farcs007$ and a source redshift of $z_s = 1.716 \pm 0.002$. Again the I-band flux ratio $f_I = 0.21$ is below the limit for our statistical lens sample. The lens redshift is ~ 0.55, estimated from colors and magnitude of the lens galaxy and mass modeling.

- SDSS J1524+4409: A two-image lens with an image separation of $\theta = 1\farcs669 \pm 0\farcs020$. The source redshift is $z_s = 1.210 \pm 0.001$, and the lens redshift is $z_l = 0.320 \pm 0.001$. In I-band the lensing galaxy is much brighter than the lensed quasar components.

We note that SDSS J0832+0404 and SDSS J1524+4409 will be included in the lens lists from the DR3 quasar catalog (Inada et al. 2007). The DR5 quasar catalog (Schneider et al. 2007) contains SDSS J1216+3529 and SDSS J1322+1052 as well, but not as lenses. The number of lensed quasars discovered (or recovered) by the SQLS is now more than 30,[2] comprising a significant fraction of all lensed quasars known.

This work was supported in part by Department of Energy contract DE-AC02-76SF00515. I. K. acknowledges support from Grant-in-Aid for Scientific Research on Priority Areas No. 467. A. C. acknowledges the support of CONICYT, Chile, under grant FONDECYT 1051061. This work is based in part on observations obtained with the Apache Point Observatory 3.5-meter telescope, which is owned and operated by the Astrophysical Research Consortium, and on data collected at Subaru Telescope, which is operated by the National Astronomical Observatory of Japan. Use of the UH 2.2-m telescope and the UKIRT for the observations is supported by NAOJ.

Funding for the SDSS and SDSS-II has been provided by the Alfred P. Sloan Foundation, the Participating Institutions, the National Science Foundation, the U.S. Department of Energy, the National Aeronautics and Space Administration, the Japanese Monbukagakusho,

[2]See http://www-utap.phys.s.u-tokyo.ac.jp/~sdss/sqls/ for a list of lensed quasars in the SQLS.

the Max Planck Society, and the Higher Education Funding Council for England. The SDSS Web Site is http://www.sdss.org/.

The SDSS is managed by the Astrophysical Research Consortium for the Participating Institutions. The Participating Institutions are the American Museum of Natural History, Astrophysical Institute Potsdam, University of Basel, Cambridge University, Case Western Reserve University, University of Chicago, Drexel University, Fermilab, the Institute for Advanced Study, the Japan Participation Group, Johns Hopkins University, the Joint Institute for Nuclear Astrophysics, the Kavli Institute for Particle Astrophysics and Cosmology, the Korean Scientist Group, the Chinese Academy of Sciences (LAMOST), Los Alamos National Laboratory, the Max-Planck-Institute for Astronomy (MPIA), the Max-Planck-Institute for Astrophysics (MPA), New Mexico State University, Ohio State University, University of Pittsburgh, University of Portsmouth, Princeton University, the United States Naval Observatory, and the University of Washington.

REFERENCES

Abazajian, K., et al. 2003, AJ, 126, 2081

Abazajian, K., et al. 2004, AJ, 128, 502

Abazajian, K., et al. 2005, AJ, 129, 1755

Adelman-McCarthy, J. K., et al. 2006, ApJS, 162, 38

Adelman-McCarthy, J. K., et al. 2007a, ApJS, 172, 634

Adelman-McCarthy, J. K., et al. 2007b, ApJS, submitted (arXiv:0707.3413)

Blanton, M. R., Lin, H., Lupton, R. H., Maley, F. M., Young, N., Zehavi, I., & Loveday, J. 2003, AJ, 125, 2276

Browne, I. W. A., et al. 2003, MNRAS, 341, 13

Chae, K.-H., et al. 2002, Phys. Rev. Lett., 89, 151301

Eisenstein, D. J., et al. 2001, AJ, 122, 2267

Falco, E. E., et al. 1999, ApJ, 523, 617

Fukugita, M., Ichikawa, T., Gunn, J. E., Doi, M., Shimasaku, K., & Schneider, D. P. 1996, AJ, 111, 1748

Fukugita, M., Shimasaku, K., & Ichikawa, T. 1995, PASP, 107, 945

Gunn, J. E., et al. 1998, AJ, 116, 3040

Gunn, J. E., et al. 2006, AJ, 131, 2332

Helbig, P., Marlow, D., Quast, R., Wilkinson, P. N., Browne, I. W. A., & Koopmans, L. V. E. 1999, A&AS, 136, 297

Hogg, D. W., Finkbeiner, D. P., Schlegel, D. J., & Gunn, J. E. 2001, AJ, 122, 2129

Inada, N. et al. 2007, AJ, in press (arXiv:0708.0828)

Ivezić, Ž., et al. 2004, AN, 325, 583

Kashikawa, N., et al. 2002, PASJ, 54, 819

Kayo, I. et al. 2007, AJ, 134, 1515

Keeton, C. R. 2001b, preprint (astro-ph/0102340)

Kochanek, C. S., Keeton, C. R., & McLeod, B. A. 2001, ApJ, 547, 50

Kochanek, C. S., Schneider, P., Wambsganss, J., 2006, Part 2 of Gravitational Lensing: Strong, Weak & Micro, Proceedings of the 33rd Saas-Fee Advanced Course, G. Meylan, P. Jetzer & P. North, eds. (Springer-Verlag: Berlin), 91

Landolt, A. U. 1992, AJ, 104, 340

Lupton, R. H., Gunn, J. E., & Szalay, A. S. 1999, AJ, 118, 1406

Lupton, R., Gunn, J. E., Ivezić, Z., Knapp, G. R., Kent, S., & Yasuda, N. 2001, in ASP Conf. Ser. 238, Astronomical Data Analysis Software and Systems X, ed. F. R. Harnden, Jr., F. A. Primini, and H. E. Payne (San Francisco: Astr. Soc. Pac.), p. 269 (astro-ph/0101420)

Lupton, R. 2007, AJ, submitted

Maoz, D., et al. 1993, ApJ, 409, 28

Myers, S. T., et al. 2003, MNRAS, 341, 1

Nelson, A. E., Gonzalez, A. H., Zaritsky, D., & Dalcanton, J. J. 2001, ApJ, 563, 629

Oguri, M., Keeton, C. R., & Dalal, N. 2005, MNRAS, 364, 1451

Oguri, M., et al. 2006, AJ, 132, 999

Oguri, M. 2007, ApJ, 660, 1

Oke, J. B. 1990, AJ, 99, 1621

Peng, C. Y., Ho, L. C., Impey, C. D., & Rix, H.-W. 2002, AJ, 124, 266

Persson, S. E., Murphy, D. C., Krzeminski, W., Roth, M., & Rieke, M. J. 1998, AJ, 116, 2475

Pier, J. R., Munn, J. A., Hindsley, R. B., Hennessy, G. S., Kent, S. M., Lupton, R. H., & Ivezić, Ź. 2003, AJ, 125, 1559

Richards, G. T., et al. 2002, AJ, 123, 2945

Rusin, D., et al. 2003, ApJ, 587, 143

Schneider, D. P., et al. 2005, AJ, 130, 367

Schneider, D. P., et al. 2007, AJ, 134, 102

Smith, J. A., et al. 2002, AJ, 123, 2121

Stoughton, C., et al. 2002, AJ, 123, 485

Strauss, M. A., et al. 2002, AJ, 124, 1810

Tucker, D. L., et al. 2006, AN, 327, 821

Uehara, M., et al. 2004, Proc. SPIE, 5492, 661

York, D. G., et al. 2000, AJ, 120, 1579

This preprint was prepared with the AAS LaTeX macros v5.2.

Table 1. SDSS Properties of Gravitationally Lensed Quasars

Name	RA	Dec	u	g	r	i	z	Redshift
SDSS J0832+0404	08:32:16.99	+04:04:05.2	19.42 ± 0.04	19.31 ± 0.02	18.98 ± 0.02	18.95 ± 0.02	18.92 ± 0.05	1.115 ± 0.003
SDSS J1216+3529	12:16:46.05	+35:29:41.5	19.56 ± 0.05	19.43 ± 0.03	19.24 ± 0.03	19.11 ± 0.04	18.85 ± 0.04	2.012 ± 0.002
SDSS J1322+1052	13:22:36.41	+10:52:39.4	19.82 ± 0.04	19.08 ± 0.02	18.75 ± 0.01	18.29 ± 0.02	18.15 ± 0.03	1.716 ± 0.002
SDSS J1524+4409	15:24:45.63	+44:09:49.6	19.94 ± 0.05	19.76 ± 0.03	19.16 ± 0.02	18.82 ± 0.02	18.49 ± 0.04	1.210 ± 0.001

Note. — Magnitudes are Point Spread Function (PSF) magnitudes without Galactic extinction correction. The PSF magnitudes roughly corresponds to magnitudes of the brighter quasar images for these lens systems.

Table 2. SDSS J0832+0404: Astrometry and Photometry

Name	ΔX[arcsec]	ΔY[arcsec]	V	I	K
A	0.000 ± 0.003	0.000 ± 0.003	18.87 ± 0.01	18.43 ± 0.01	16.82 ± 0.01
B	-1.579 ± 0.005	-1.202 ± 0.005	20.75 ± 0.02	20.08 ± 0.08	17.70 ± 0.02
G	-1.292 ± 0.008	-0.875 ± 0.008	$\cdots$	19.35 ± 0.03	16.06 ± 0.01

Note. — The positive directions of ΔX and ΔY are defined by West and North, respectively. The errors are statistical errors only, and do not include systematic errors such as model uncertainties, template PSF uncertainties, and zero-point errors. The positions are derived in K-band image.

Table 3. SDSS J1216+3529: Astrometry and Photometry

Name	ΔX[arcsec]	ΔY[arcsec]	V	R	I	H
A	0.000 ± 0.002	0.000 ± 0.002	18.97 ± 0.01	18.85 ± 0.01	18.36 ± 0.01	17.30 ± 0.01
B	1.486 ± 0.002	0.097 ± 0.002	19.95 ± 0.01	19.82 ± 0.01	19.33 ± 0.01	18.20 ± 0.03
G1	0.931 ± 0.033	-0.075 ± 0.033	$\cdots$	21.58 ± 0.06	20.31 ± 0.05	18.15 ± 0.06
G2	1.743 ± 0.022	2.891 ± 0.022	$\cdots$	21.79 ± 0.08	20.79 ± 0.05	19.23 ± 0.13

Note. — See Table 2 for a note. The positions are derived in I-band image.

Table 4. SDSS J1322+1052: Astrometry and Photometry

Name	ΔX[arcsec]	ΔY[arcsec]	V	R	I	H
A	0.000 ± 0.002	0.000 ± 0.002	18.71 ± 0.01	18.41 ± 0.01	17.75 ± 0.01	16.48 ± 0.01
B	1.052 ± 0.004	1.702 ± 0.004	20.50 ± 0.02	20.19 ± 0.01	19.47 ± 0.01	18.04 ± 0.02
G	0.714 ± 0.018	1.169 ± 0.018	22.09 ± 0.10	20.55 ± 0.04	19.67 ± 0.03	17.17 ± 0.02

Note. — See Table 2 for a note. The positions are derived in I-band image.

Table 5. SDSS J1524+4409: Astrometry and Photometry

Name	ΔX[arcsec]	ΔY[arcsec]	B	R	I
A	0.000 ± 0.008	0.000 ± 0.008	20.61 ± 0.03	19.98 ± 0.02	19.54 ± 0.04
B	-1.485 ± 0.012	0.761 ± 0.012	21.36 ± 0.05	20.57 ± 0.02	20.17 ± 0.03
G	-0.576 ± 0.012	0.142 ± 0.012	21.80 ± 0.07	19.06 ± 0.02	18.33 ± 0.01

Note. — See Table 2 for a note. The positions are derived in I-band image.

Table 6. Mass Modeling

Name	$R_{\rm Ein}$	e	θ_e[deg]	$\mu_{\rm tot}$	$\Delta t[h^{-1}{\rm day}]$
SDSS J0832+0404	$0\farcs95$	0.28	+17	3.1	157.8
SDSS J1216+3529	$0\farcs77$	0.15	−55	8.4	15.6
SDSS J1322+1052	$1\farcs03$	0.18	−33	7.3	45.5
SDSS J1524+4409	$0\farcs79$	0.29	−40	7.4	15.3

Note. — For SDSS J1216+3529 and SDSS J1322+1052, we assume the lens redshift of $z_l = 0.5$ in computing predicted time delays.

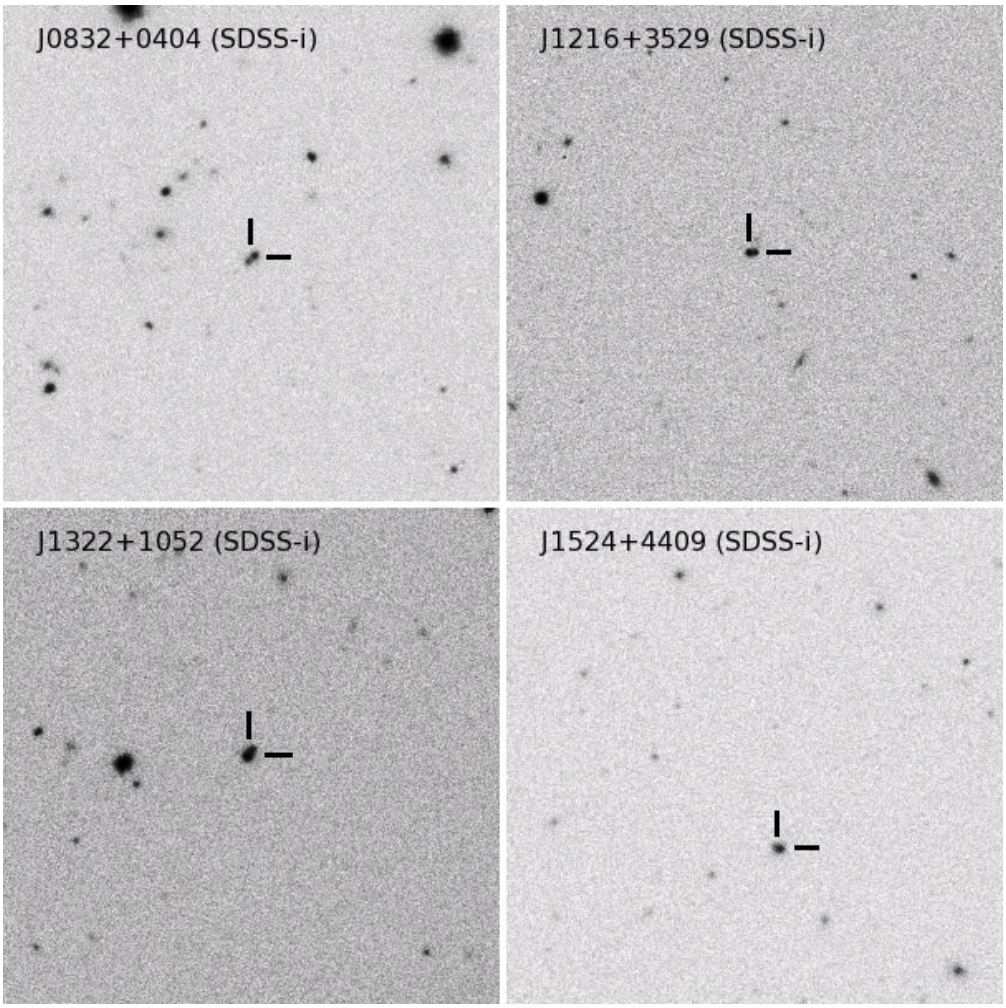

Fig. 1.— Wide-field SDSS i-band images of four new lensed quasars, SDSS J0832+0404 (*upper left*), SDSS J1216+3529 (*upper right*), SDSS J1322+1052 (*lower left*), and SDSS J1524+4409 (*lower right*). The size of each image is $2' \times 2'$. North is up and East is left.

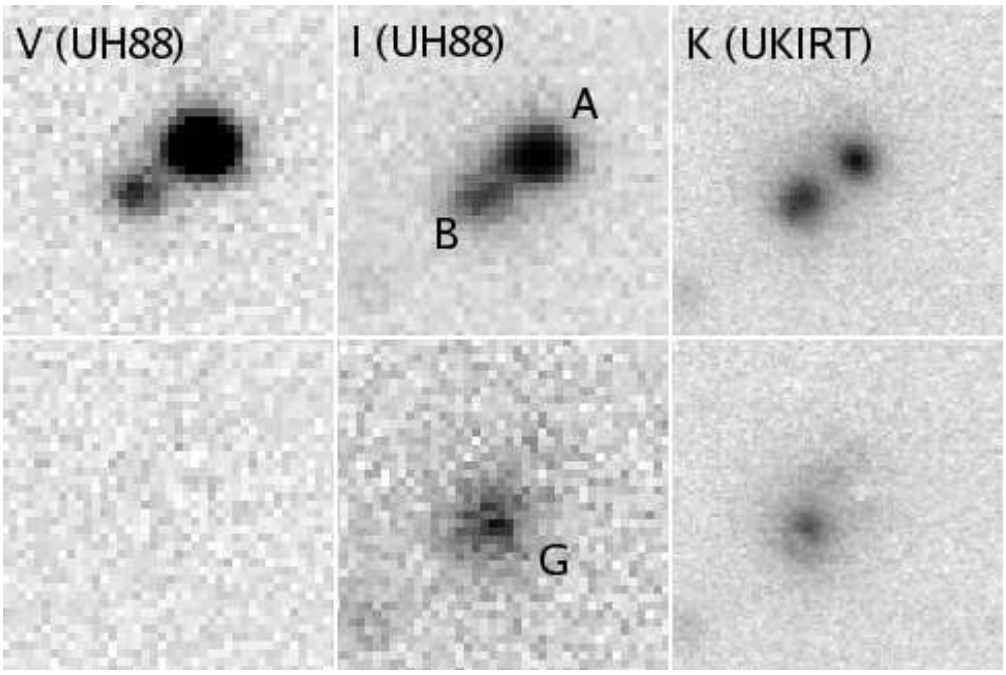

Fig. 2.— Images of SDSS J0832+0404 taken with Tek2k at the UH88 telescope (V and I) and UFTI at UKIRT (K). The upper panels show original images, and the bottom panels show residuals after subtracting two stellar (quasar) components; here the lens galaxy is seen more clearly. North is up and East is left, and the size of each image is $8\farcs8 \times 8\farcs8$. The results are summarized in Table 2.

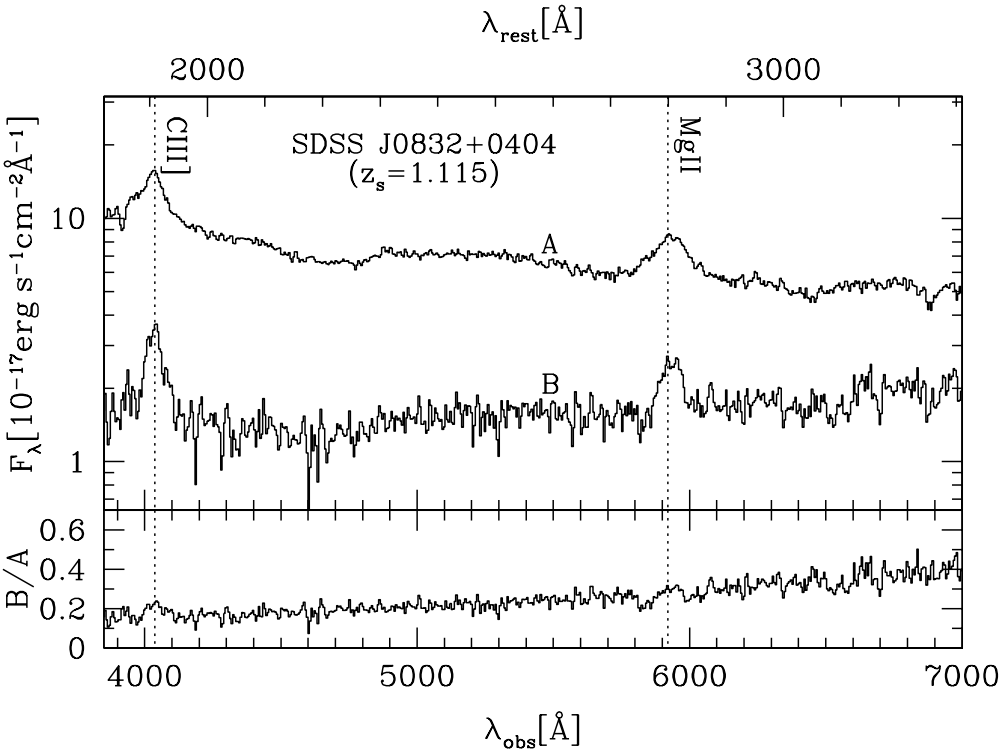

Fig. 3.— Spectra of SDSS J0832+0404 A and B(+G) taken with EFOSC2 at the ESO3.6m telescope. The spectral resolution is $R \sim 400$. Dotted lines indicate quasar emission lines redshifted to $z_s = 1.115$. The lower panel plots the ratio of the two spectra.

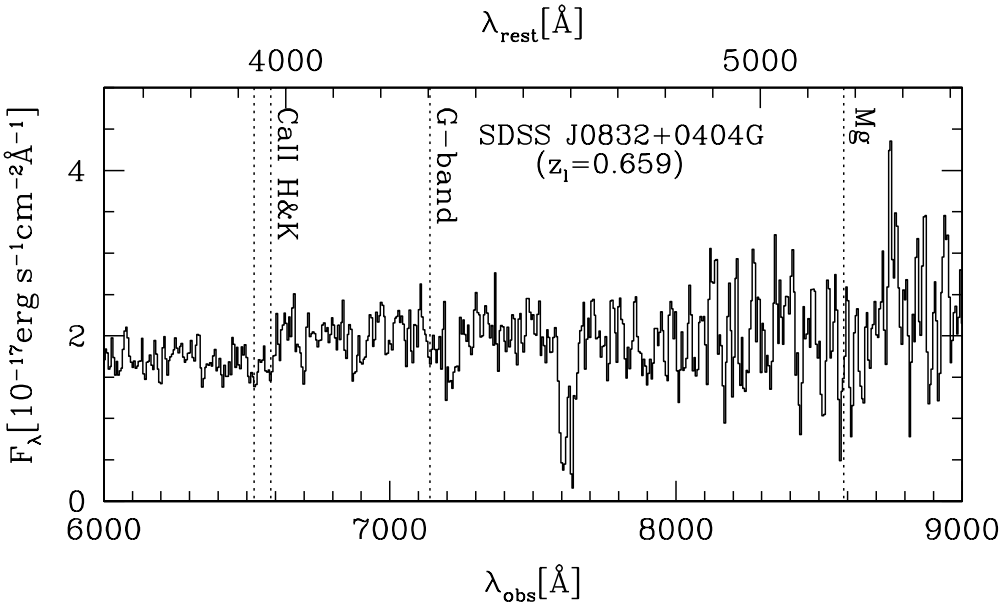

Fig. 4.— The expanded view of the spectrum of SDSS J0832+0404 B (Figure 3) that shows an indication of the lens galaxy. The break at $\sim 6600\,\text{Å}$ and two adjacent absorption lines suggests that the lens redshift of this system is $z_l = 0.659$. The strong absorption at $\sim 7600\,\text{Å}$ is telluric.

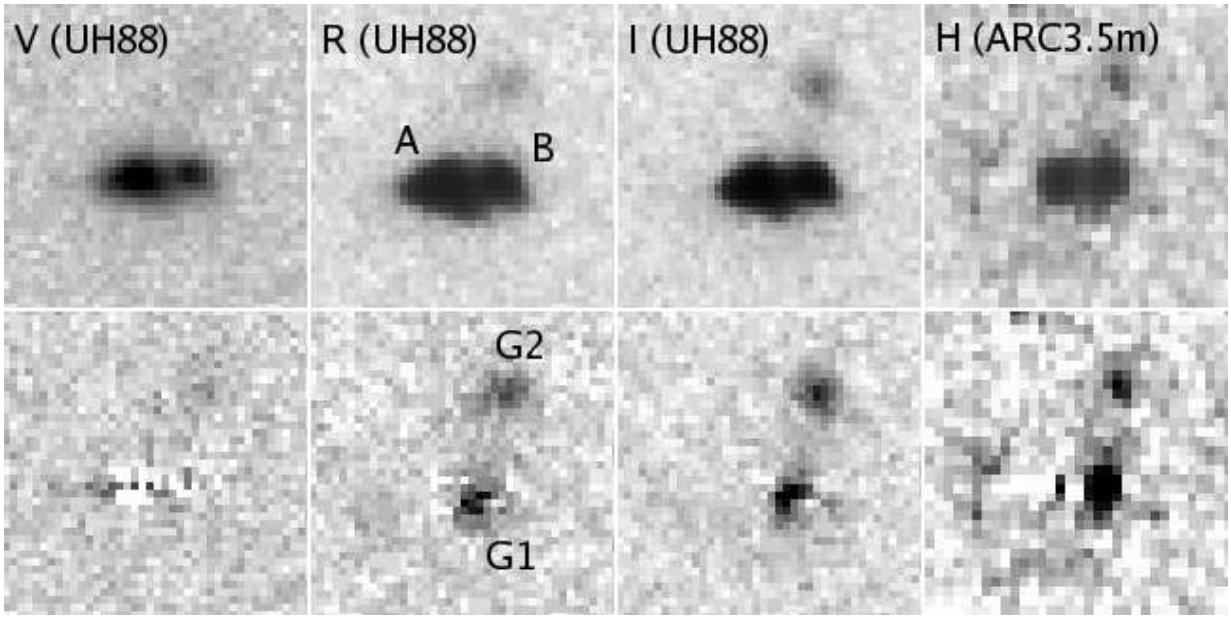

Fig. 5.— Images of SDSS J1216+3529 taken with Tek2k at the UH88 telescope (V, R, and I) and NIC-FPS at the ARC3.5m telescope (H). As in Figure 2, upper and lower panels show original images and residuals after subtracting two stellar (quasar) components, respectively. North is up and East is left, and the size of each image is $8\farcs8 \times 8\farcs8$. The results are summarized in Table 3.

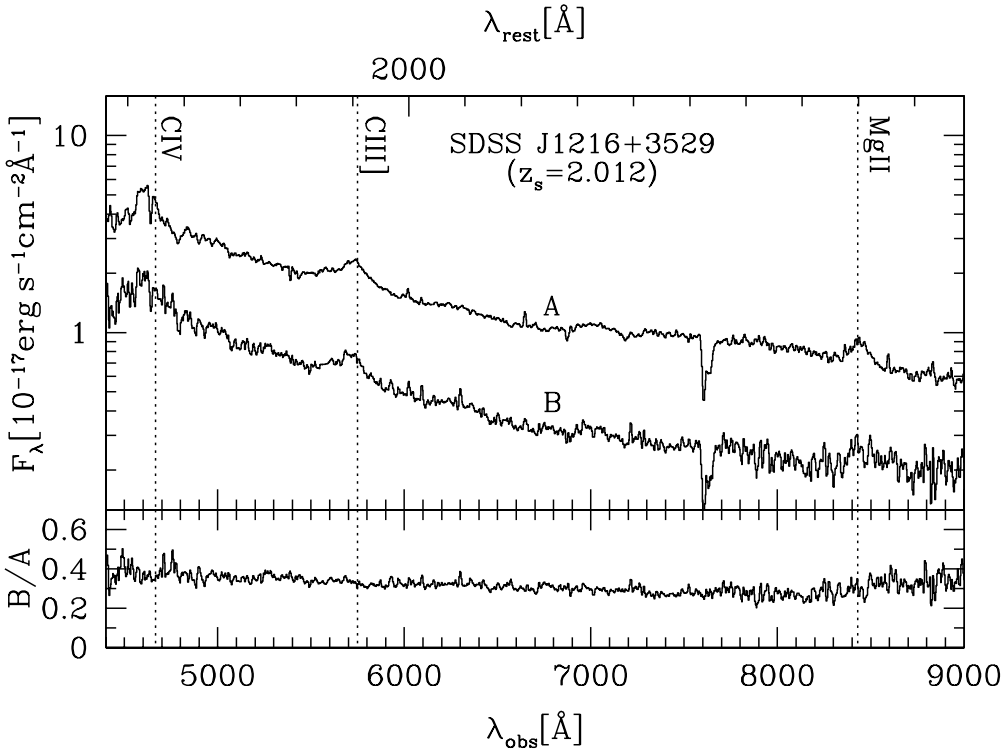

Fig. 6.— Spectra of SDSS J1216+3529 A and B taken with WFGS2 at the UH88 telescope. The spectral resolution is $R \sim 700$. The spectra are smoothed with a 3-pixel boxcar. The location of quasar emission lines redshifted to $z_s = 2.012$ is indicated by vertical dotted lines. The lower panel plots the ratio of the two spectra. The feature at ~ 7600 Å is telluric.

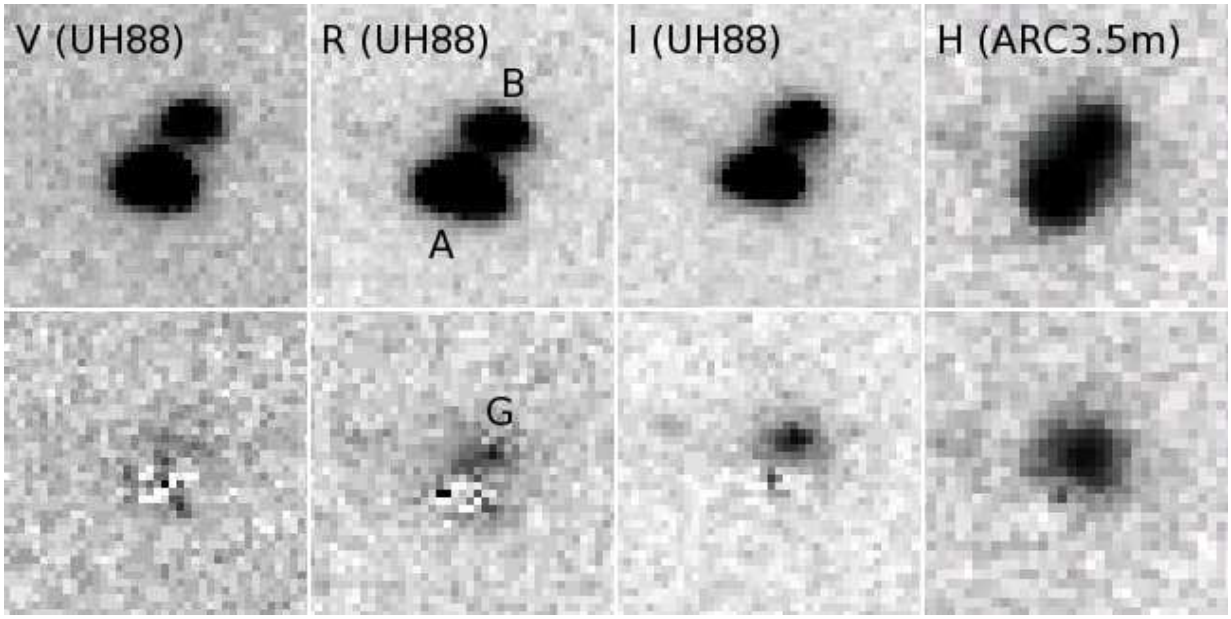

Fig. 7.— Images of SDSS J1322+1052 taken with Tek2k at the UH88 telescope (V, R, and I) and NIC-FPS at the ARC3.5m telescope (H). As in Figure 2, upper and lower panels show original images and residuals after subtracting two stellar (quasar) components, respectively. North is up and East is left, and the size of each image is $8\farcs8 \times 8\farcs8$. The result is summarized in Table 4.

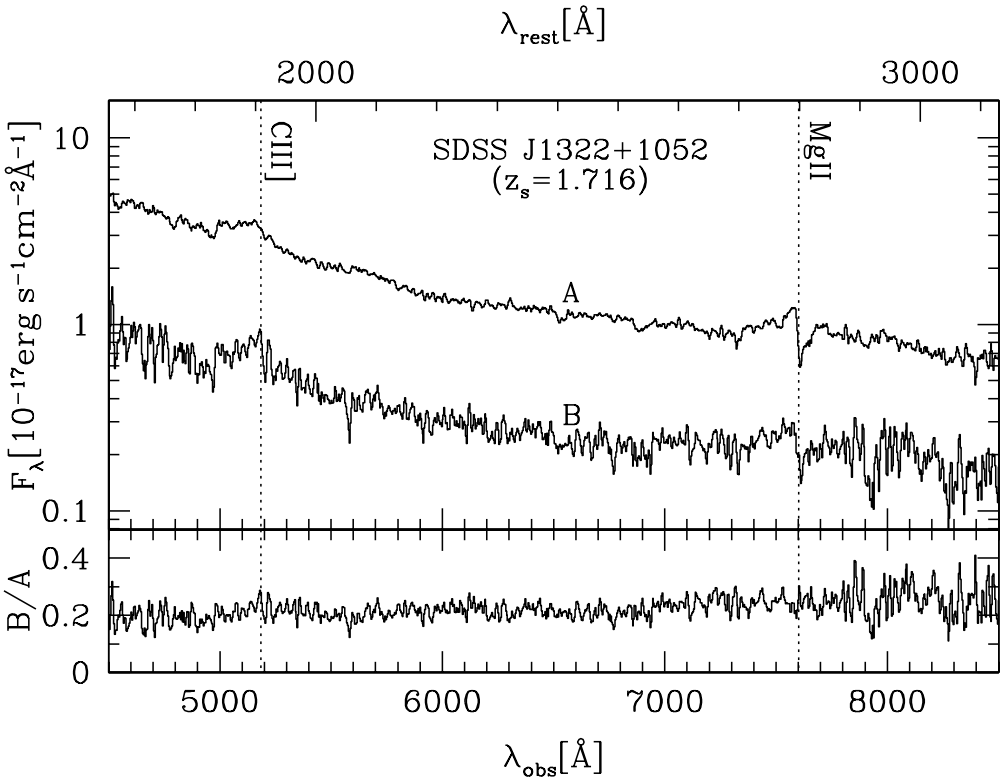

Fig. 8.— Spectra of SDSS J1322+1052 A and B taken with WFGS2 at the UH88 telescope. The spectral resolution is $R \sim 700$. The spectra are smoothed with a 3-pixel boxcar. Vertical lines indicate quasar emission lines redshifted to $z_s = 1.716$. Note that the Mg II emission lines are contaminated by telluric absorption at ~ 7600 Å. The lower panel plots the ratio of the two spectra.

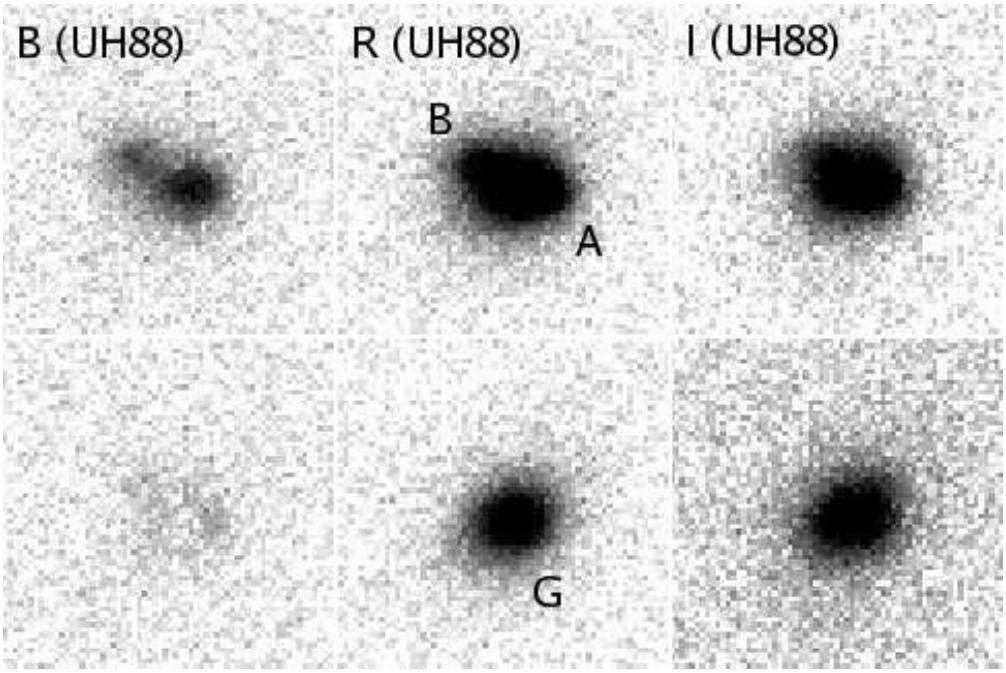

Fig. 9.— Images of SDSS J1524+4409 taken with OPTIC at the UH88 telescope (B, V, and I). As in Figure 2, upper and lower panels show original images and residuals after subtracting two stellar (quasar) components, respectively. North is up and East is left, and the size of each image is $8\farcs8 \times 8\farcs8$. The result is summarized in Table 5.

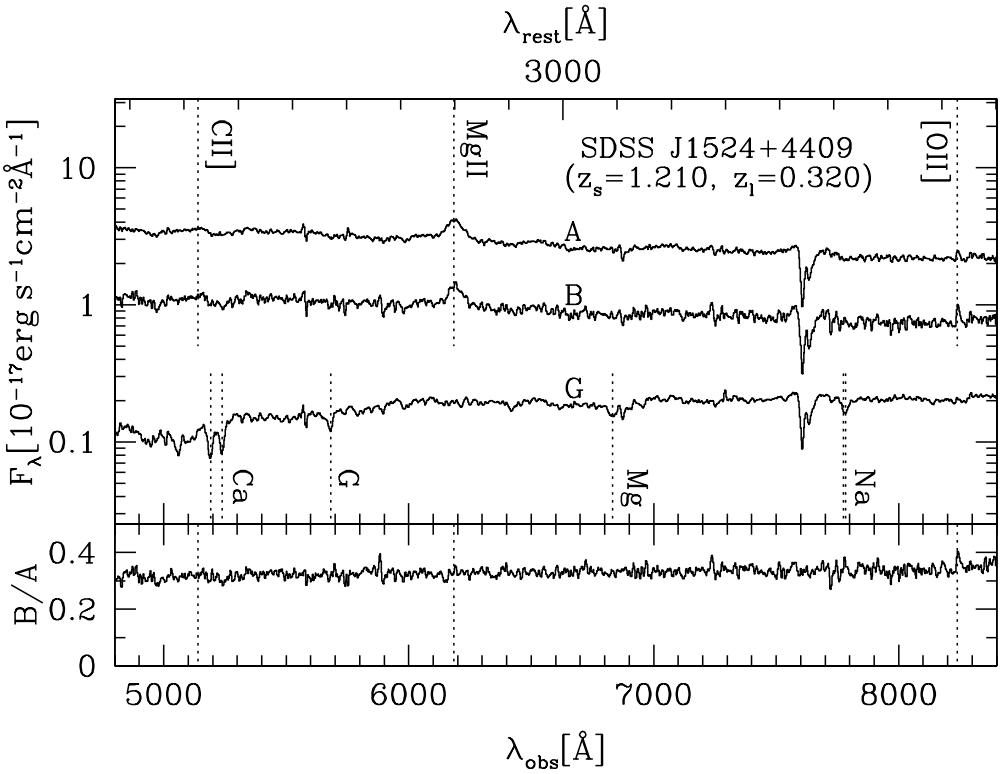

Fig. 10.— Spectra of SDSS J1524+4409 A, B, and G taken with FOCAS at the Subaru telescope. The spectral resolution is $R \sim 500$. All the spectra are smoothed with a 3-pixel boxcar. The spectrum of galaxy G is shifted downward for illustrative purpose. Both quasar emission lines redshifted to $z_s = 1.210$ and galaxy absorption lines redshifted to $z_l = 0.320$ are indicated with vertical dotted lines. The feature at ~ 7600 Å is telluric. The lower panel plots the ratio of the spectra of components A and B.